The Ring-Opening Reaction of Chromenes: A Photochemical Mode-Dependent Transformation

Annapaola Migani,[†] Pier Luigi Gentili,[‡] Fabrizia Negri,*[,§] Massimo Olivucci,*[,†,||] Aldo Romani,[‡] Gianna Favaro,*[,‡] and Ralph S. Becker[⊥]

Dipartimento di Chimica, Università di Siena, 53100 Siena, Italy, Dipartimento di Chimica, Università di Perugia, Via Elce di Sotto 8, 06123 Perugia, Italy, Dipartimento di Chimica, Università di Bologna, Via Selmi 2, 40126 Bologna, Italy, Centro per lo Studio dei Sistemi Complessi, Università di Siena, via Pendola 37, Siena, Italy, and Centro de Quimica Estrutural, Instituto Superior Tecnico, 1049-001 Lisbon, Portugal

Received: June 6, 2005; In Final Form: August 4, 2005

The efficiency of the photochemical ring-opening of chromenes (or benzopyrans) depends on the vibronic transition selected by the chosen excitation wavelength. In the present work, ab initio CASPT2//CASSCF calculations are used to determine the excited-state ring-opening reaction coordinate for 2H-chromene (C) and 2,2-diethyl-2H-chromene (DEC) and provide an explanation for such an unusual mode-dependent behavior. It is shown that excited-state relaxation and decay occur via a multimodal and barrierless (or nearly barrierless) reaction coordinate. In particular, the relaxation out of the Franck−Condon involves a combination of in-plane skeletal stretching and out-of-plane modes, while the second part of the reaction coordinate is dominated exclusively by a different out-of-plane mode. Population of this last mode is shown to be preparatory with respect to both C−O bond breaking and decay via an S_1/S_0 conical intersection. The observed mode-dependent ring-opening efficiency is explained by showing that the vibrational mode corresponding to the most efficient vibronic transition has the largest projection onto the out-of-plane mode of the reaction coordinate. To support the computationally derived mechanism, we provide experimental evidence that the photochemical ring-opening reaction of 2,2-dimethyl-7,8-benzo(2H)chromene, that similarly to DEC exhibits a mode-dependent photoreaction, has a low (∼1 kcal mol^{-1}) activation energy barrier.

1. Introduction

For several years, chemists have been making efforts to understand molecular dynamics. More and more detailed images of molecular motions are being depicted by means of theoretical studies and experimental data collected using time-resolved spectroscopic techniques. Single molecules appear as dynamic entities provided with ordered movements. For the latter purpose, monochromatic light becomes an effective tool. For example, during the past decades[1] many experiments have been carried out wherein polyatomic molecules in the gas phase were vibronically excited by laser light, varying the degree and nature of internal activation. The general picture that is emerging entails a first step that involves the absorption of light by specific molecular modes[2−4] and a second step where energy randomization can compete with useful reactive processes. If the time scale for randomization is shorter than that of the progression along the reactive path, the reaction will be mode-independent. If, in contrast, such a progression competes or is faster than intramolecular vibrational redistribution (IVR) and/or with intermolecular energy transfer (IET), a mode-dependent reaction[5−11] is expected to occur.

An intriguing example on this subject observed in the condensed phase (and not in gas phase) comes from a class of photochromic compounds, the chromenes, whose photobehavior is represented in Scheme 1. The photochromism of these compounds was discovered[12−17] in the 1960s and has recently been the subject of a review.[18] In the absence of UV light, they exist in the closed, uncolored form. Upon UV irradiation, the C_2−O bond breaks, and the open, colored form is produced. In fluid media at room temperature, the bleaching to the closed structure occurs thermally and photochemically. Since the closed forms have a rigid molecular framework, they exhibit electronic absorption bands with fairly resolved vibrational structures, especially at low temperatures in glassy matrices. The effect of selective excitation at different vibronic levels on their photobehavior was established in previous works.[19−22] Generally, the fluorescence quantum yield (Φ_F) decreases and the reaction quantum yield (Φ_{PC}) increases by increasing the vibronic level at which the molecule is excited. However, the quantum yields are not simply linear functions of the excitation energy, but they are strongly dependent on the nature of the vibronic mode that is excited. A vibrational analysis of the absorption spectra showed the involvement of two main optically active modes: one between 280 and 380 cm^{-1} and the other between 1300 and 1400 cm^{-1}, depending on the molecular structure.[19−22] Despite the lower degree of internal energy, the lower-frequency mode, in general, is more efficient in giving the product than the higher frequency mode. The observation of a dependence of Φ_F and Φ_{PC} on the excitation wavelength suggests the existence of an S_1 barrierless (or nearly barrierless) path connecting the photoproduct to a real crossing (a conical intersection)[23,24] between S_1 and S_0. In this case, the reaction

* E-mail: olivucci@unisi.it, favaro@unipg.it, fabrizia.negri@unibo.it.
† Dipartimento di Chimica, Università di Siena.
‡ Università di Perugia.
§ Università di Bologna.
|| Centro per lo Studio dei Sistemi Complessi, Università di Siena.
⊥ Instituto Superior Tecnico.

10.1021/jp052996b CCC: $30.25
Published on Web 09/13/2005

SCHEME 1

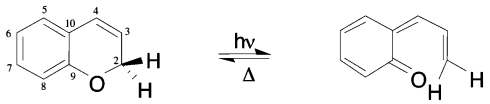

SCHEME 2

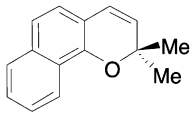

quantum yield and the nuclear velocity can be related by the Landau Zener formula,[25] which correlates faster nuclear dynamics toward the crossing to higher Φ_{PC} values. In other words, upon decay at the conical intersection, the branching depends on the amount of kinetic energy in the reactive degrees of freedom pointing toward the photoproduct. This type of model has been successfully applied to the cis−trans isomerization in rhodopsin photoreceptors (see ref 26), the correlation between quantum yield and reaction speed,[27] and the wavelength dependence of the quantum yield.[11]

These observations raise some important questions: What is the nature of the two optically active modes? What is the geometric relationship between the active vibrations and the photochemical reaction coordinate? In view of this relationship, is it possible to understand why different vibrations exhibit a different photochemical efficiency?

The aim of this work is to provide a mechanistic model for the interpretation of the mode-dependent photobehavior of chromenes based on ab initio quantum chemical calculations. A CASSCF study of the first excited state (S_1) for 2H-chromene (C) has already been reported.[28] The results demonstrate that the ring-opening reaction coordinate is characterized by a transition state connecting a cyclic intermediate to an acyclic structure corresponding to a conical intersection between the S_1 and ground state (S_0) energy surfaces. Relaxation from the conical intersection on the ground-state surface leads to production of the first open form (ortho-quinodal with cisoid geometry) or back conversion to the closed form. In the present study, a careful analysis of the minimum energy path (MEP) along the S_1 ring-opening coordinate of C and 2,2-diethyl-2H-chromene (DEC) has been carried out within the framework of the higher-level CASPT2//CASSCF computations.[29] For both C and DEC, the vibrational frequencies and activities in the $S_0 \rightarrow S_1$ transition have been determined by assuming the Franck−Condon (FC) mechanism as the main source of intensity.[30] Hence, the assigned most optically active modes have been correlated with the modes involved in the S_1 MEP in order to rationalize the different efficiency in giving the open form.

CASPT2//CASSCF computations have also been employed to determine the height of the energy barrier[31] controlling S_1 decay and product formation. The results have been assessed experimentally for 2,2-dimethyl-7,8-benzo(2H)chromene (7,8-DMBC) (Scheme 2) by determining the reaction quantum yield at a specific excitation wavelength as a function of the temperature.

2. Materials and Methods

2.1. Computational Methods. The photochemical ring-opening reaction paths of C and DEC have been computed using fully unconstrained ab initio quantum chemical computations in the framework of a CASPT2//CASSCF strategy.[29] This

SCHEME 3

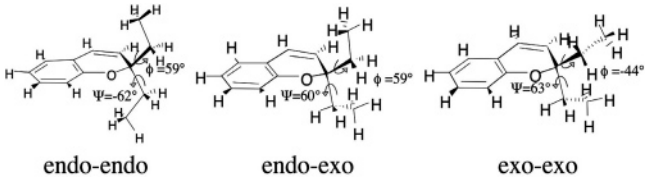

endo-endo endo-exo exo-exo

requires that the reaction coordinate is computed at the CASSCF level of theory (using the methodologies available in the *Gaussian 98*[32] series of programs) and that the corresponding energy profile is reevaluated at the multiconfigurational second-order Møller−Plesset perturbation theory level (using the CASPT2 method implemented in MOLCAS-5[33]) to take into account the effect of electron dynamic correlation. More specifically, the CASSCF S_1 excited MEP reaction coordinate computations were performed using the 6-31G* basis set and an active space of 12 electrons in 11 orbitals including the benzene π/π^* orbitals, the oxygen atom lone pair (n) perpendicular to the average plane defined by the annular molecular skeleton, the C═C double bond π/π^* orbitals, and the C−O bond σ/σ^* orbitals. The single-point CASPT2 computations were performed along a selected number of MEP points using a three-root (S_2, S_1, S_0) state-average (0.33, 0.33, 0,33) CASSCF zeroth-order wave function with a 12e/11o complete active space and the 6-31G* basis set. The detailed procedure adopted to carry out the MEP computations is reported in ref 34.

To simulate the vibronic intensities, the ground and first excited state equilibrium geometries for compounds C and DEC along with the vibrational frequencies at the excited-state equilibrium geometry have been computed. These computations have been carried out at the same level of theory (CASSCF-(12e/11o)/6-31G*) adopted to map the excited-state ring-opening reaction coordinate. The vibrational frequencies have been obtained by means of numerical frequency calculations. Although intensity borrowing mechanisms may contribute in some frequency regions of the absorption spectra of these molecules, the FC mechanism has been assumed as the main source of intensity.[30] This is reasonable owing to the reduced symmetry of the molecules and especially true, as will be seen, for the two modes that influence their photochemical behavior. According to this mechanism, the simulation of vibronic intensities has been carried out by extracting from the S_0 and S_1 equilibrium structures and S_1 force field the displacement parameters $B_{S0,S1}$ which govern the vibronic structure of the $S_0 \rightarrow S_1$ transition as described, for instance, in ref 30. A Lorentzian line of 10 cm^{-1} has been associated with each computed vibronic transition. No scaling of the vibrational frequencies was applied.

As illustrated in Scheme 3, DEC exists in three possible conformations (exo−exo, endo−exo, endo−endo) that can be interconverted by rotation of the two ethyl groups. The nomenclature used refers to the dihedral angles ϕ and ψ. The endo−endo conformer is the least stable because of steric hindrance between the two eclipsed ethyl groups (see Table 1 discussed below). We computed the excited-state reaction coordinate for the exo−exo conformer. For the computation of the vibronic intensities, we used the endo−exo conformer. Note that the excited-state coordinate and vibronic intensities are not expected to depend on whether the conformation is exo−exo, endo−exo, or endo−endo. Throughout the text, the nomenclature that denotes the conformer will be omitted.

2.2. Experimental Methods. 7,8-DMBC was synthesized by Carlos Gartner (Harvard University, U.S.A.) and was used without further purification. The solvent, 3-methylpentane

TABLE 1: Absolute CASSCF and Absolute and Relative CASPT2//CASSCF Energies for C and DEC

structure	state	CASSCF energy (hartree)	CASPT2 energy (hartree)	relative energy CASPT2 (kcal mol^{-1})	expt (nm)	theory (nm)	oscillator strenght
			2H-Chromene (C)				
FC[c]	S_0	(−420.43948)					
	S_0	−420.43539[b]	−421.67028	0.0[a]			
	S_1	−420.26515[b]	−421.51645	96.53	314 (max)[e]	296	0.015
	S_2	−420.19507[b]	−421.44898	138.87	267 (max)[e]	206	0.004
M[c]	S_1	(−420.27639)					
	S_0	−420.42607[b]	−421.66157	5.47			
	S_1	−420.27462[b]	−421.52536	90.94			
	S_2	−420.21262[b]	−421.45840	132.96			
TS[c]	S_1	(−420.26780)					
	S_0	−420.40359[b]	−421.64381	16.61			
	S_1	−420.26410[b]	−421.53089	87.47			
	S_2	−420.21783[b]	−421.49221	111.74			
CI[d]	S_0	(−420.34024)					
	S_1	(−420.34019)					
	S_0	−420.34147[b]	−421.57429	60.24			
	S_1	−420.33707[b]	−421.58603	52.87			
	S_2	−420.26175[b]	−421.51995	94.34			
			2,2-Diethyl-2H-chromene (DEC)				
exo−exo S_0 minimum = **FC**[c]	S_0	(−576.57702)		[0.0][g]			
	S_0	−576.57285[b]	−578.35663	0.0[a]			
	S_1	−576.40313[b]	−578.20371	95.96	311 (max)[f]	298	0.019
	S_2	−576.33337[b]	−578.13112	141.51	266 (max)[f]	202	0.007
exo−exo exo−exo S_1 minimum = **M**[c]	S_1	(−576.41413)					
	S_0	−576.56376[b]	−578.34850	5.10			
	S_1	−576.41230[b]	−578.21271	90.31			
	S_2	−576.35003[b]	−578.14398	133.44			
TS[c]	S_1	(−576.40579)					
	S_0	−576.54145[b]	−578.33141	15.83			
	S_1	−576.40168[b]	−578.21881	86.48			
	S_2	−576.35491[b]	−578.18268	93.33			
CI[d]	S_0	(−576.47754)					
	S_1	(−576.47731)					
	S_0	−576.47922[b]	−578.26150	59.70			
	S_1	−576.47352[b]	−578.27590	50.66			
	S_2	−576.40324[b]	−578.20969	92.21			
endo−exo S_0 minimum[c]	S_0	(−576.58358)		[−4.12]			
endo−endo S_0 minimum[c]	S_0	(−576.58395)		[−4.35]			

[a] For each model, energies are relative to the S_0 state energy of the S_0 minimum. [b] S_0, S_1, and S_2 state-average energies (weights 0.33, 0.33, and 0.33).The three-root state-average CASSCF wave functions correspond to the zeroth-order wave functions for the CASPT2 computations. [c] Geometry optimized with single-root CASSCF wave function. [d] Geometry optimized with S_1 and S_0 state-average CASSCF wave function (weights 0.5, 0.5). [e] From ref 36. [f] From ref 19.

(3MP), a reagent-grade Acros product, was distilled before use. The absorption spectra were recorded using a Hewlett-Packard 8453 diode-array spectrophotometer. The 7,8-DMBC reaction quantum yield was determined in the 230−270 K temperature range by exciting at 354 nm, which corresponds to the lowest energy vibronic peak maximum of the $S_0 \rightarrow S_1$ transition. A 125 W Xe lamp, filtered by a Jobin-Yvon H10 UV monochromator (16 nm band-pass) and focused on the sample (in a fluorimetric 1-cm-path cell) by a silica fiber optic, was used as an irradiating source. The irradiation was carried out at a right angle with respect to the monitoring beam of the spectrophotometer. The radiation intensity was determined using potassium ferrioxalate actinometry. The absorbed photon density was on the order of 10^{-7} moles of photons dm^{-3} s^{-1} at the irradiation wavelength. The 7,8-DMBC concentration was on the order of 5×10^{-5} mol dm^{-3}. The color-forming process was followed at various analysis wavelengths (430, 450, and 473 nm) in order to estimate the Φ_{PC} values with more accuracy. The initial rate method was applied using the open form molar absorption coefficients (ϵ_P), previously determined in a 3MP matrix.[35]

3. Results and Discussion

3.1. The S_1 Ring-Opening Reaction Coordinate of C and DEC. Table 1 presents the CASSCF absolute and CASPT2 absolute and relative energy data for both the investigated chromenes. Only CASPT2 (i.e., the more accurate) energy data will be discussed in the text. The computed vertical excitation energy data can be used to validate the methodology reported in subsection 2.1. Experimentally, compound C in *n*-hexane generates two electronic bands with maxima at 314 and 267 nm.[36] These data compare fairly well with the computed first vertical excitation energy (296 nm) yielding ca. 5 kcal mol^{-1} errors and only approximately with the second vertical excitation energy (206 nm). Similarly, the predicted values for the $S_0 \rightarrow S_1$ and $S_0 \rightarrow S_2$ (with S_2 we indicate the second excited state) vertical excitation energies of DEC (298 and 202 nm, respectively) are in reasonable agreement with the experimental $S_0 \rightarrow S_1$ and $S_0 \rightarrow S_2$ transition maxima observed in 3MP (311 and 266 nm, respectively).[19] The calculations show that the $S_0 \rightarrow S_1$ transitions of C and DEC correspond to weak transitions (the oscillator strengths are 0.015 and 0.019, respectively) and

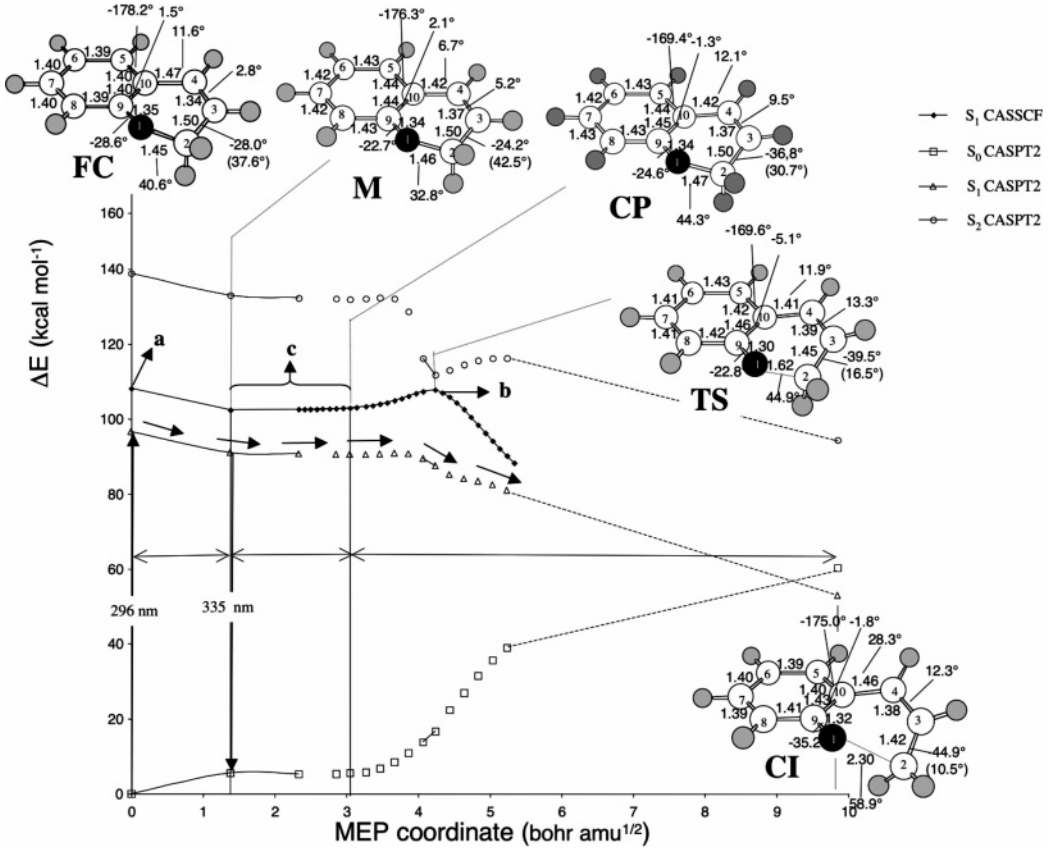

Figure 1. Energy profiles along the S_1 MEP describing the ring-opening reaction coordinate of C. The structures (geometrical parameters in Å and deg) document the geometrical change along the coordinate. The stream of arrows on the S_1 surface represents the reaction path.

the $S_0 \rightarrow S_2$ transitions correspond to very weak transitions (the oscillator strengths are 0.004 and 0.007, respectively).

The six π-electrons of benzene together with the two π-electrons of the C_3-C_4 bond and the couple of electrons located in the perpendicular oxygen n-orbital define an extended chromophore. The S_1 vertical transition determines the population of orbitals having antibonding character for the benzene ring and the C_3-C_4 bond and with bonding character for the $C_{10}-C_4$ bond. Note that, as described below, this type of excitation is consistent with the early geometrical distortion of the system.

Figures 1 and 2 report the S_2, S_1, and S_0 energy profiles along the S_1 MEP describing the ring-opening reaction coordinate of C and DEC. These energy profiles show the following: (i) The S_1 reaction path is substantially barrierless; (ii) the S_1 and S_0 surfaces come progressively together and ultimately reach a conical intersection where S_1 and S_0 are completely degenerate; (iii) a S_2/S_1 avoided crossing exists along the S_1 ring-opening coordinate.

The following discussion refers to C unless otherwise stated. Inspection of Figure 1 shows that the initial acceleration driving the system out of the **FC** region is dominated by skeletal stretching that involves symmetric expansion of the benzene ring coupled with some inversion of the character of the two adjacent C_4-C_{10} and C_3-C_4 bonds of the pyran moiety. This motion leads to an excited-state minimum (**M**) located only 5.5 kcal mol^{-1} below **FC**. The **FC** $\rightarrow$ **M** distortion is similar to that described by the forces acting on the **FC** structure shown in Figure 3 (labeled a in Figure 1). The skeletal stretching is mixed with the out-of-plane mode. Notice that these molecular motions are responsible for the largest vibronic activities observed and computed for the absorption spectra (see also next section). The molecule becomes more planar during the **FC** $\rightarrow$ **M** relaxation: the $C_9-O_1-C_2-C_3$ dihedral angle changes from 40.6° to 32.8°. In particular, the $C_9-O_1-C_2-C_3$, $O_1-C_2-C_3-C_4$, and $C_9-C_{10}-C_4-C_3$ become significantly less twisted (by 8°, 4°, and 5°, respectively), while the changes of $O_1-C_9-C_{10}-C_4$ and $C_{10}-C_4-C_3-C_2$ are smaller and in the opposite direction (1° and 2° more twisted). On the whole, the change favors a more planar structure.

The contribution of the out-of-plane mode becomes dominant when the system enters an energy plateau. In fact, from inspection of the CASPT2 energy profile in Figure 1, it can be seen that there is only limited change in energy from **M** up to the transition-state point **TS** (this point is defined by the top of the barrier located along the corresponding CASSCF profile). To analyze the structural change that characterizes the energy plateau region, it is useful to consider its central point (**CP**) located at ca. 3 au along the reaction coordinate. Note that at **CP** the C_2-C_3, C_2-O_1, and C_9-O_1 bond lengths are unchanged relative to the excited-state minimum **M** (1.50, 1.46, and 1.34 Å respectively). Thus, at **M**, the skeletal stretching is completed, and the reaction coordinate becomes dominated by the out-of-plane mode. In particular, the molecule becomes more puckered along the **M** $\rightarrow$ **CP** path segment as shown by the value of the $C_9-O_1-C_2-C_3$ parameter that changes from 32.8° to 44.3°.

The data reported in Figure 1 also show that the deformation along the $C_9-O_1-C_2-C_3$ ring-puckering mode is coupled with the $H-C_2-C_3-H$ torsion. The $H-C_2-C_3-H$ parameter measures the rotation of the H at C_2 (here we consider the equatorial hydrogen) relative to that of the H at C_3, thus monitoring the steric repulsion between the two CH groups. It can be seen that the $H-C_2-C_3-H$ torsion increases from 37.6° to 42.5° and decreases from 42.5° to 30.7° on going from **FC** to **M** to **CP**,

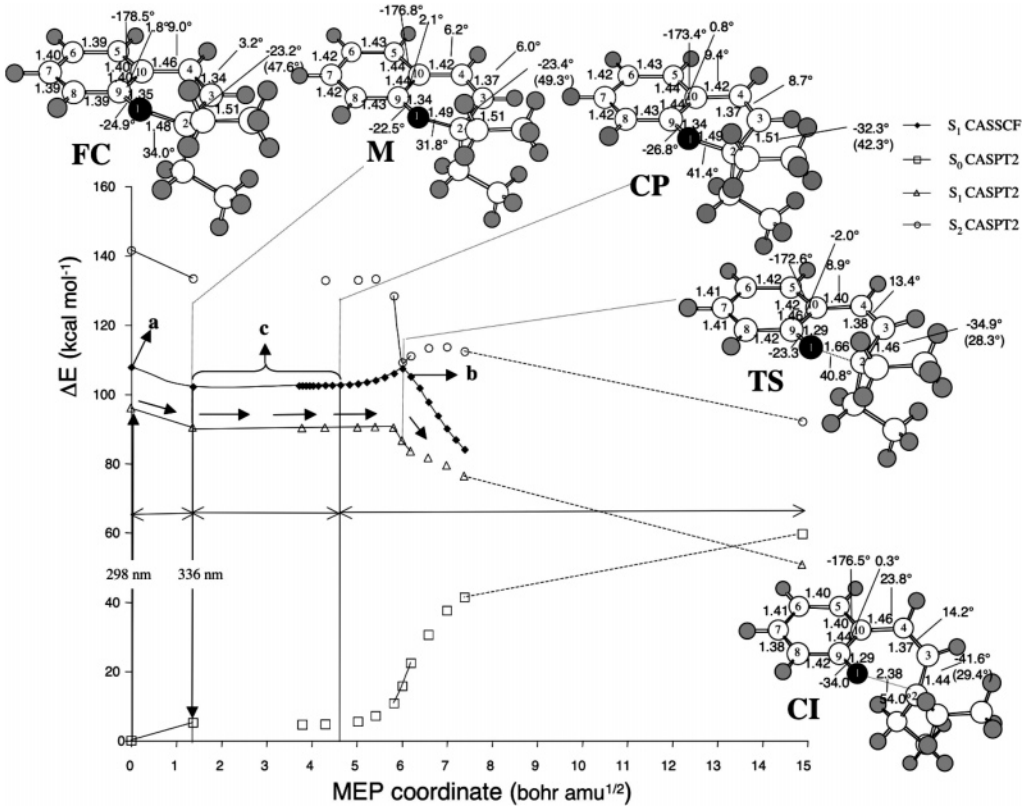

Figure 2. Energy profiles along the S_1 MEP describing the ring-opening reaction coordinate of DEC. The structures (geometrical parameters in Å and deg) document the geometrical change along the coordinate. The stream of arrows on the S_1 surface represents the reaction path.

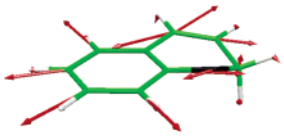

a

Figure 3. Forces at the **FC** geometry on S_1 (labeled a in Figure 1).

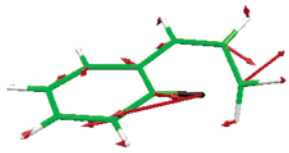

b

Figure 4. Forces at one selected structure belonging to the terminal part of the computed relaxation coordinate (labeled b in Figure 1).

respectively. Thus, we found for the H−C_2−C_3−H torsion an oscillatory behavior similar to that reported for the C_9−O_1−C_2−C_3 torsion.

In the **FC** → **M** domain, the out-of-plane mode is responsible for a flattening of the molecule. As a result, at point **M** the C_2−O_1 bond features an unfavorable orientation to interact with the π-system. The following **M** → **CP** change can be considered *preparatory* for the population of the C_2−O_1 bond-breaking mode. In fact, in this domain the out-of-plane deformation twists the C_2−O_1 σ bond with respect to the ring plane and forces it into a position more parallel to the π-system, thus facilitating the $\sigma\pi$ interactions required to trigger the C_2−O_1 bond-breaking. The **CP** point marks the separation between the region of the reaction coordinate dominated by the out-of-plane mode and that dominated by the C_2−O_1 breaking coordinate. Figure 1 shows that, beyond this point, the reaction coordinate is dominated by the increase of the C_2−O_1 bond length (from 1.47 to 2.30 Å) and decrease of the C_2−C_3 and C_9−O_1 bond lengths (from 1.50 to 1.42 and 1.34 and 1.32 Å, respectively). In Figure 4, we have plotted the gradient vector for one selected structure belonging to the terminal part of the computed relaxation coordinate (labeled b in Figure 1). This vector, consistent with the change described in Figure 1, has the large component corresponding to the C_2−O_1 bond elongation accompanied by C_2−C_3 and C_9−O_1 compression.

The C_2−O_1 bond-breaking mode leads directly to a S_1/S_0 conical intersection structure (**CI**) located 43 kcal mol^{-1} lower than **FC**. **CI** provides a fully efficient S_1 → S_0 radiationless decay channel, and it is characterized by the crossing of the S_1 n−π* and S_0 potential energy surfaces of the system. The same type of conical intersection has been documented in other cases such as for *s-cis*-acrolein.[37] Since at **M** the electronic structure of S_1 still corresponds to that of a π−π* excited state, a change from π−π* to n−π* must occur along the **M** → **CI** segment of the reaction coordinate. Indeed, as shown in Figure 1, this change of electronic structure is associated with the existence of a S_1/S_2 avoided crossing along the ring-opening coordinate and in correspondence of the **TS** structure.

Comparison between Figures 1 and 2 shows that the inclusion of two ethyl groups in DEC does not affect the pattern of the computed reaction coordinate but favors a less puckered structure. In fact, at the **FC** point, the C_9−O_1−C_2−C_3 dihedral angle is 40.6° in the parent molecule (see Figure 1) and 34.0° in the DEC exo−exo conformer, while the H−C_2−C_3−H (Et−C_2−C_3−H) angle is 37.6° in C compared to 47.6° in the substituted compound. In general, we observe an increase of molecular rigidity: Deformation along the out-of-plane mode is less pronounced in the substituted compound relative to the parent molecule along the entire reaction coordinate. This seems

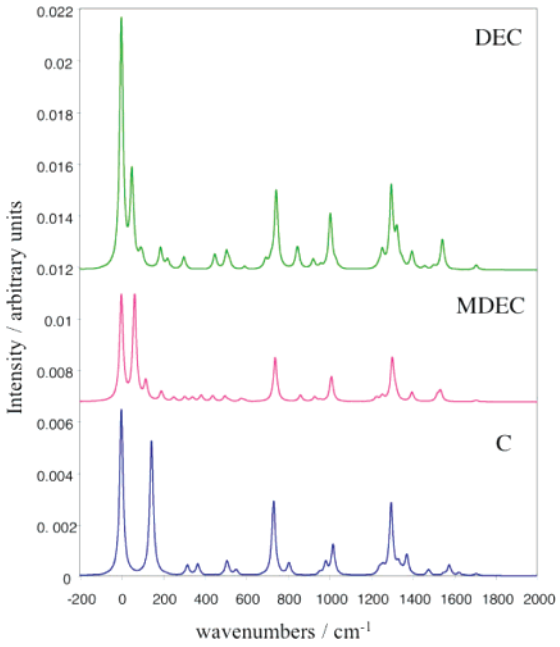

Figure 5. Simulation of the absorption spectra of C, MDEC, and DEC (Lorentzian line width 10 cm^{-1}, only FC activities are considered).

related to a minimization of steric hindrance or can be explained by the increase in the reduced mass of the substituted system.

3.2. Vibronic Effects in C and DEC. As mentioned above for C only, a poorly resolved absorption spectrum has been reported.[36] In the case of DEC, the vibrational analysis of the $S_0 \rightarrow S_1$ transition shows that there are two active vibrations of ~280 and ~1300 cm^{-1}.[19] Our aim is to identify the nature of these active vibrations and establish the relationship between them and the geometrical change along the reaction coordinate. We performed three simulations evaluating the vibronic intensities of C and DEC and of a chromene model (MDEC) where the two ethyl groups were not included explicitly but approximated by 29 amu point masses. The results of these three simulations are compared in Figure 5 (see also Table S1 in the Supporting Information).

According to the FC mechanism, activity is predicted for those vibrations that overlap with the early distortion of the system (**FC** → **M** domain of the reaction coordinate). Thus, we expect to find the largest vibronic activities for modes corresponding to the initial excited-state relaxation discussed in the previous section: skeletal stretching and out-of-plane modes. In Figure 6, the most active vibrations for C are shown. Very high FC activity is indeed predicted in the low-frequency region associated with the 145 cm^{-1} mode that corresponds to a ring-puckering. The 1298 cm^{-1} mode is the second most FC active vibration corresponding to a stretching motion with large amplitude on the C_4-C_{10} and C_3-C_4 bonds. Further, in this vibration, there is a large component of methylene twisting. The 1298 cm^{-1} vibration is closely related to the S_1 forces at the **FC** point (see in Figure 3) that display a large component of C_3-C_4 expansion. Our simulations also predict a large and modest activity for two planar bending vibrations at 733 and 1019 cm^{-1}, respectively.

Note that the 1374 cm^{-1} mode (Figure 7a) that has a large component of $C_9-O_1-C_2$ asymmetric stretching and methylene twisting, and therefore describes the type of distortion required to reach the S_1/S_0 conical intersection (see Figure 4), is only very weakly FC active.

The results relative to the simulation of FC activities for DEC show no substantial differences in the high-frequency region

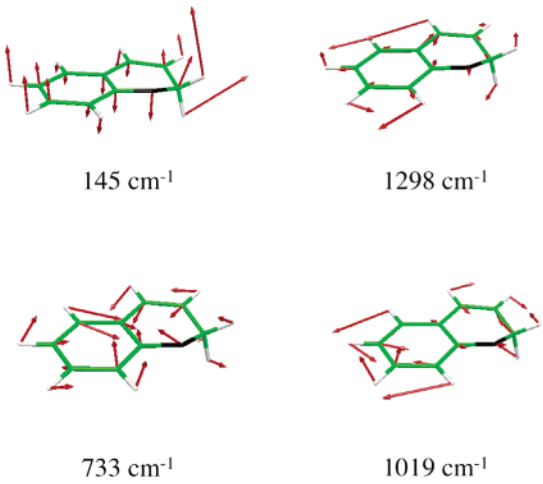

Figure 6. Comupted FC active vibrational modes for C corresponding to the 145, 733, 1019, and 1298 cm^{-1} vibrational frequencies.

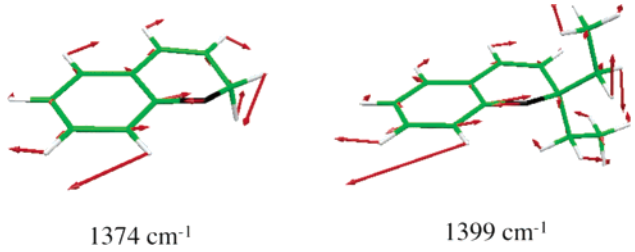

Figure 7. Molecular motion associated with the 1374 cm^{-1} vibrational frequency of C and the 1399 cm^{-1} vibrational frequency of DEC.

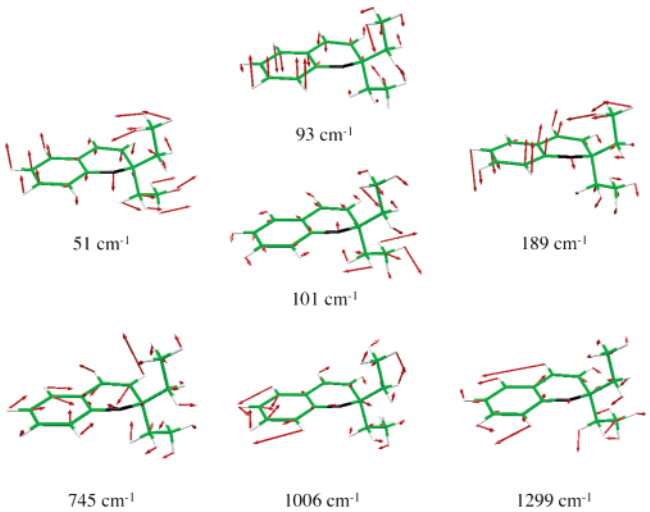

Figure 8. Comupted FC active vibrational modes for DEC corresponding to the 51, 93, 101, 189, 745, 1006, and 1299 cm^{-1} vibrational frequencies.

of the spectrum, with the largest activities predicted for two bending vibrations at 745 and 1006 cm^{-1} that correlate with the 733 and 1019 cm^{-1} modes of the parent molecule and the C_3-C_4 stretching mode at 1299 cm^{-1} correlating with 1298 cm^{-1} vibration of C.

In Figure 8, we show the molecular motions associated with the active vibrations of the substituted molecule. Similarly to the parent molecule, a modest activity is predicted for the 1399 cm^{-1} mode (Figure 7b) that bears a large component of $C_9-O_1-C_2$ asymmetric stretching coupled to a twisting of the two ethyl substituents.

Some differences between C and DEC are found in the low-frequency region of the spectrum (0−300 cm^{-1}). While in C

TABLE 2: Most Relevant Dushinsky Coefficients Representing the Mode Mixing of the Three Lowest-Frequency Modes (S_1 State) of MDEC in Terms of the S_1 State Normal Modes of Compound C

C frequencies		MDEC frequencies		
	cm^{-1}	64	118	192
1	137	−0.37	0.73	0.14
2	145	0.56	0.46	−0.43
3	217	0.24	0.07	0.83
4	318	0.09	−0.05	0.06
6	384	−0.10		
7	451	−0.09		

the activity is concentrated in one individual out-of-plane mode at 145 cm^{-1}, in DEC the activity is spread over four out-of-plane vibrations at 51, 93, 101 and 188 cm^{-1}. In particular, the calculations predict considerable intensity for the 51 cm^{-1} mode and almost equally small intensities for the 93, 101, and 188 cm^{-1} vibrations. To rationalize the different low-frequency intensity distributions, we evaluated the Dushinsky mode-mixing matrices[38] between the normal modes of C and MDEC (MDEC is taken as a simplified model of DEC). Notice that the use of MDEC instead of DEC is meaningful, since the spectrum simulated for MDEC is very similar to that obtained for DEC, with marked or modest activity predicted in the low-frequency region at 64, 118, and 192 cm^{-1} and in the high-frequency region at 740, 1011, 1304, and 1399 cm^{-1}. Furthermore, note that the deviations of the vibrational frequencies of MDEC from those computed for DEC do not exceed 10 cm^{-1}.

The most relevant MDEC−C mode-mixing coefficients for the three lowest-frequency modes of MDEC are listed in Table 2. It is shown that the 145 cm^{-1} mode of C contributes to approximately the same extent to the vibrational modes of frequencies 64, 118, and 192 cm^{-1} of MDEC. Accordingly, the intensity that is concentrated at 145 cm^{-1} in C becomes distributed across the 64, 118, and 192 cm^{-1} modes in MDEC. Similarly, as observed above, in DEC we found that the intensity is distributed among the low-frequency 51, 93, 101, and 188 cm^{-1} modes that correlate with the 64, 118, and 192 cm^{-1} vibrations of MDEC. Unfortunately, the simulations concentrate most of the activity on the lowest-frequency mode at 51 cm^{-1}, in contrast with the experimental spectra where intensity dominates at 280 cm^{-1}. In this regard, we notice that the harmonic approximation employed here to simulate FC intensities is less adequate for the low-frequency modes whose energy profile often deviates remarkably from the harmonic potential. For this reason, we deem less accurate the intensities computed for the low-frequency vibrations, and among these, the one most affected by inaccuracies is the mode at 51 (64) cm^{-1}, whose intensity may be artificially overestimated.

The simulations presented in Figure 5 suggest the following assignments for the active vibrations of DEC:[19]

(I) The activity of the 1300 cm^{-1} mode is supported by our computations that predict the 1299 cm^{-1} band to be one of the most prominent in the spectrum. This mode, which had been previously assigned to the C−O stretching,[21] is instead attributed to a skeletal stretching with large amplitude on the C_3-C_4 bond. The frequency of the vibration deviates from the experimental value by only 1 cm^{-1}.

(II) Our simulations predict activity in the low-frequency region associated with out-of-plane motions in agreement with the experimental data. On the basis of the above discussion, we tentatively assign the band observed experimentally at 280 cm^{-1} to the 188 cm^{-1} vibrational mode of DEC and (192 cm^{-1} of MDEC) that, as shown in Figure 8, has a large component of ring-puckering. The computed frequency underestimation can be partially attributed to the out-of-plane nature of this mode, which makes its force constant very strongly dependent on the level of theory employed.

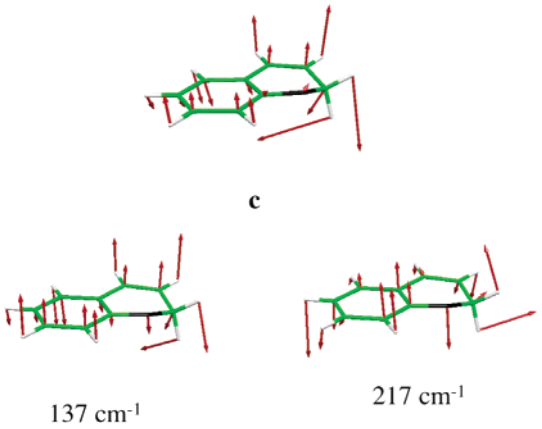

Figure 9. Comparison between patterns of vectors representing the geometry difference between points **M** and **CP** (labeled c in Figure 1) and the first (137 cm^{-1}) and third (217 cm^{-1}) lowest-frequency vibrational modes computed at **M** for **C**. The second (145 cm^{-1}) lowest-frequency vibration is shown in Figure 6. Note that the 137 and 217 cm^{-1} vibrations are not FC active.

(III) The experimentally undetected contribution of the 745 and 1006 cm^{-1} bending modes could be hidden by other bands (e.g., progressions of the low-frequency mode and combinations of the low- and high-frequency modes.)

In conclusion, the simulation of vibronic intensities reveals that the activity observed in the experimental absorption spectrum of DEC is dominated by the modes associated with the initial excited-state relaxation, namely, a high-frequency in-plane π-system skeletal stretching mode together with a low-frequency out-of-plane ring-puckering mode.

3.3. Relationship Between the Reaction Coordinate and Active Vibrational Modes. On the basis of the pattern of the computed excited-state reaction coordinate and assignment of FC active vibrations, we now attempt to explain why population of the two optically active modes shall increase the efficiency of the ring-opening reaction and why the low-frequency mode is more efficient than the high-frequency mode. A vector representation of the structural change corresponding to the geometry difference between structures **M** and **CP** is provided in Figure 9 (labeled c in Figure 1). Vector **c** clearly shows that the geometrical change along the second domain of the reaction coordinate corresponds to an out-of-plane deformation. This deformation is likely to originate from a motion similar to that described by the first three lowest frequencies corresponding to 137, 145, and 217 cm^{-1} computed at **M.** The 145 cm^{-1} mode is given in Figure 6 and, as discussed above, is FC active. The modes associated with the 137 and 217 cm^{-1} frequencies are shown in Figure 9. The projection of the **M** → **CP** vector onto the normal modes computed at **M** shows that the out-of-plane deformation has components along the 137 cm^{-1} (60%), 145 cm^{-1} (24%), and 217 cm^{-1} (16%) modes. Thus, the projection clearly shows that the most active 145 cm^{-1} mode does overlap with the **M** → **CP** domain of the reaction coordinate. As a consequence, excitation of this mode is predicted to increase the reaction efficiency (i.e., altering the back-cyclization/ring-opening branching ratio upon decay at **CI**), since the light energy is funneled along the **M** → **CP** coordinate that is preparatory to the C−O bond-breaking mode (these modes may be highly

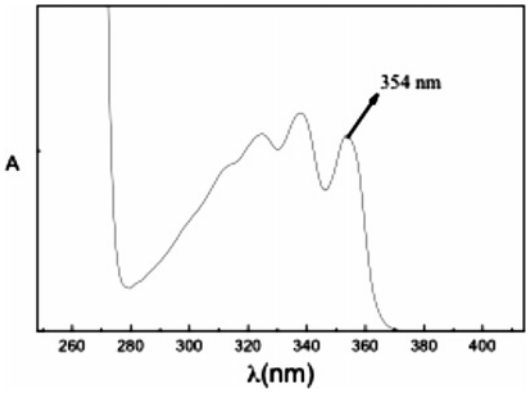

Figure 10. Absorption spectrum of 7,8-DMBC in 3MP at room temperature.

coupled through the apparent increase in overlap of the C−O σ-orbitals with the orbitals of the electronically excited π-system).

As discussed above, the vibrational motions that can be activated by absorption of light are a low-frequency (145 cm^{-1}) ring-puckering mode and a high-frequency (1298 cm^{-1}) mode. The **M → CP** reaction coordinate domain that is preparatory to C−O bond breakage shows some overlap only with the FC active 145 cm^{-1} mode and no overlap with the FC active 1298 cm^{-1} mode. This observation alone explains why the low-frequency mode is more efficient in inducing the ring-opening reaction than the high-frequency mode. On the other hand, in the case of 1298 cm^{-1} mode, it is reasonable to expect that the light energy stored in this vibration will be easily and preferentially transferred into the low-frequency mode, since these two modes are highly coupled through the reaction coordinate (as demonstrated by the fact that the early distortion of the system in the **FC → M** domain correlates with a combination of the high- and low-frequency modes). Thus, an increase of Φ_{PC} is also observed when the high-frequency mode is excited, although to a minor extent since part of the energy will be dispersed in nonreactive molecular motions other than the out-of-plane mode and therefore will be wasted.

3.4. Experimental Determination of the Energy Barrier. As mentioned in the Introduction, one basic condition required to observe mode-dependent photochemistry is that the photochemical process be ultrafast and therefore characterized by a barrierless reaction coordinate. The absence of a barrier on S_1 should prevent the occurrence of an energy randomization process that would cause a depletion of the energy stored in those vibrations that lead to an increase of the reaction efficiency. Figures 1 and 2 show that the excited-state reaction coordinates of C and DEC are barrierless or have a small energy barrier (indeed, the methodology used cannot exclude the presence of a small, <1 kcal mol^{-1} barrier in this region). This result has been validated experimentally by measuring the activation energy barrier for the ring-opening reaction of 7,8-DMBC that, similarly to DEC, exhibits a mode-dependent photoreaction.[35]

The absorption spectrum of 7,8-DMBC recorded in 3MP at room temperature is reported in Figure 10. The determination of the energy barrier has been carried out by measuring Φ_{PC} as a function of the temperature (230−270 K) at a fixed excitation wavelength (354 nm). For 7,8-DMBC, this excitation leads to population of the lowest vibrational levels of S_1. The corresponding quantum yield values are reported in Table 3.

From inspection of the table, it is apparent that there are not appreciable variations of Φ_{PC} within the degree of accuracy of the quantum yield determinations. Considering that the accuracy is within 10%, the reaction activation energy should be less than 1 kcal mol^{-1}, in line with the computational results. Therefore, the reaction can be considered to be barrierless. A low-energy barrier has also been found for another chromene, i.e., 2,2-dimethyl-5,6-benzo(2H)chromene.[39] Finally, the proposed mechanism is also supported by recent time-resolved spectroscopic studies of the photoinduced dynamics of three chromenes (2,2-spiro-adamantyl-7,8-benzo(2H)chromene, 2,2-diphenyl-(2H)chromene, and 2,2-diphenyl-5,6-benzo(2H)chromene).[40] It has been shown that the breakage of the C−O bond occurs within a few hundred femtoseconds, producing a short-lived transient that evolves to the open form having a ortho-quinoidal structure with a cisoid geometry in less than one picosecond and then to the metastable opened form with a transoid geometry within a few picoseconds. The observed sub-picosecond time scale is entirely consistent with the potential energy surfaces reported in Figures 1 and 2 that involve a barrierless coordinate leading to a conical intersection between the S_0 and S_1 potential energy surfaces.

TABLE 3: Reaction Quantum Yields, Φ_{PC}, of 7,8-DMBC (see Scheme 2) as a Function of the Temperature

T (K)	Φ_{PC}
230	0.89 ± 0.04
240	0.84 ± 0.04
250	0.86 ± 0.04
260	0.84 ± 0.04
270	0.83 ± 0.04

4. Conclusion

The results presented above provide, for the first time, a computationally based explanation of the unusual mode-dependent photochemical efficiency of chromenes. CASPT2//CASSCF calculation are used to show that the C and DEC chromenes, when excited to S_1, follow a multimode and barrierless (or nearly barrierless) reaction coordinate. Relaxation out of the **FC** region occurs along a skeletal stretching of the π-system coupled to a ring-puckering mode (out-of-plane mode). Once the skeletal stretching is completed, the reaction coordinate becomes dominated by the out-of-plane mode. Motion along this mode is *preparatory* to activate the C_2-O_1 bond-breaking mode required to reach the conical intersection between S_1 and S_0. (That is, the C_2-O_1 bond becomes more parallel to the π-system. In this way, bond expansion is triggered, ultimately leading to bond breakage with concomitant change of the electronic nature of the S_1 excited state from $\pi-\pi^*$ to $n-\pi^*$.)

The quantum yield dependence on the degree of excitation of two optically active modes at a low and high frequency is interpreted by showing that the low-frequency mode has the largest projection onto the reactive out-of-plane mode of the reaction coordinate that triggers the C−O bond-breaking process, while the high-frequency mode mainly corresponds to the unreactive skeletal stretching mode characterizing the initial part of the reaction coordinate. Thus, the maximum efficiency of the photochemical reaction is achieved when the energy is deposited in the low-frequency mode.

Finally, the computations described above reveal that the mode-dependent photobehavior is made possible by a very low, or completely absent, energy barrier separating the excited-state molecules from the product. If the excited-state molecules had to overcome a high activation barrier, energy randomization and dispersion processes would occur more rapidly than any chemical transformation. Only with a low barrier or a barrierless

reaction path can the time scale of the reactive structural change become competitive with any energy degradation process. In support of our theoretical model, we also provide experimental evidence that the activation energy barrier for the ring-opening reaction of 7,8-DMBC (that similarly to DEC exhibits a mode-dependent photoreaction) is less than 1 kcal mol^{-1}.

Acknowledgment. Funds have been provided by the Università di Siena (Progetto di Ateneo 02/04) and HFSP (RG 0229/2000-M) and in part by the MURST and the University of Perugia in the framework of the Programmi di Ricerca di Interesse Nazionale (Photoprocesses of interest for applications). Contributions from a project by young researchers (Photoinduced Processes; Study of electronic and vibronic excitation effects on reactive and radiative relaxation processes of organic molecules of the class of chromenes) is acknowledged. We thank CINECA and INSTM for granted calculation time.

Supporting Information Available: Twelve pages including computational details for Franck−Condon activity computations (Table S1), reaction coordinate analysis of $C_9-O_1-C_2-C_3$ and $H-C_2-C_3-H$ ($Et-C_2-C_3-H$) torsions (Figure S1), and 14 tables containing the Cartesian coordinates for the CASSCF/6-31G* optimized geometries discussed in the text. This material is available free of charge via the Internet at http://pubs.acs.org.

References and Notes

(1) Reisler, H.; Wettig, C. *Annu. Rev. Phys. Chem.* **1986**, *37*, 307−349.
(2) Bixon, M.; Jortner, J. *J. Chem. Phys.* **1968**, *48*, 715−726.
(3) Lin, S. H. *J. Chem. Phys.* **1966**, *44*, 3759−3767.
(4) Robinson, G. W.; Frosch, R. P. *J. Chem. Phys.* **1962**, *37*, 1962−1973.
(5) Bishenden, E.; Donaldson, D. J. *J. Chem. Phys.* **1993**, *99*, 3129−3132.
(6) Bishenden, E.; Donaldson, D. J. *J. Chem. Phys.* **1994**, *101*, 9565−9572.
(7) Courtney, S. H.; Balk, M. W.; Philips, L. A.; Webb, S. P.; Yang, D.; Levy, D. H.; Fleming, G. R. *J. Chem. Phys.* **1988**, *89*, 6697−6707.
(8) Fidder, H.; Tschirschwitz, T.; Dühr, O.; Nibbering, E. T. J. *J. Chem. Phys.* **2001**, *114*, 6781−6794.
(9) Kholmanskii, A. S. *Russ. J. Phys. Chem.* **1983**, *53*, 413−416.
(10) Kiermeier, A.; Kühlewind, H.; Neusser, H. J.; Schlag, E. W.; Lin, S. H. *J. Chem. Phys.* **1988**, *88*, 6182−6190.
(11) Kim, J. E.; Tauber, M. J.; Mathies, R. A. *Biochemistry* **2001**, *40*, 13774−13778.
(12) Becker, R. S.; Michl, J. *J. Am. Chem. Soc.* **1966**, *88*, 5931−5933.
(13) Becker, R. S.; Kolc, J. *J. Phys. Chem.* **1968**, *72*, 997−1001.
(14) Kolc, J.; Becker, R. S. *J. Phys. Chem.* **1967**, *71*, 4045−4048.
(15) Kolc, J.; Becker, R. S. *Photochem. Photobiol.* **1970**, *12*, 383−393.
(16) Kolc, J.; Becker, R. S. *J. Chem. Soc., Perkin Trans. 2* **1972**, *2*, 17.
(17) Lenoble, C.; Becker, R. S. *J. Photochem.* **1986**, *33*, 187−197.
(18) Van Gemert, B. In *Organic Photochromic and Thermochromic Compounds*; Crano, J. C., Guglielmetti, R. J., Eds.; Plenum Press: New York, London, 1999; Vol. 1.
(19) Becker, R. S.; Dolan, E.; Balke, D. E. *J. Chem. Phys.* **1969**, *50*, 239−245.
(20) Becker, R. S.; Pelliccioli, A. P.; Romani, A.; Favaro, G. *J. Am. Chem. Soc.* **1999**, *121*, 2104−2109.
(21) Favaro, G.; Romani, A.; Becker, R. S. *Photochem. Photobiol.* **2001**, *74*, 378−384.
(22) Gentili, P. L.; Romani, A.; Becker, R. S.; Favaro, G. *Chem. Phys.* **2005**, *309*, 167−175.
(23) Bernardi, F.; Olivucci, M.; Robb, M. A. *Chem. Soc. Rev.* **1996**, 321−328.
(24) Michl, J.; Bonacic-Koutecky, V. *Electronic Aspects of Organic Photochemistry*; Wiley: New York, 1990.
(25) Desouter-Lecomte, M.; Lorquet, J. C. *J. Chem. Phys.* **1979**, *71*, 4391−4403.
(26) Wang, Q.; Schoenlein, R. W.; Peteanu, L. A.; Mathies, R. A.; Shank, C. V. *Science* **1994**, *266*, 422−424.
(27) Mathies, R. A.; Lugtenburg, J. In *Handbook of Biological Physics*; Stavenga, D. G., de Grip, W. J., Pugh, E. N., Eds.; Elsevier Science B. V.: Amsterdam, 2000; Vol. 3, pp 55−90.
(28) Celani, P.; Bernardi, F.; Olivucci, M.; Robb, M. A. *J. Am. Chem. Soc.* **1997**, *119*, 10815−10820.
(29) Gonzales-Luque, R.; Garavelli, M.; Bernardi, F.; Merchán, M.; Robb, M. A.; Olivucci, M. *Proc. Natl. Acad. Sci. U.S.A.* **2000**, *97*, 9379−9384.
(30) Negri, F.; Zgierski, M. Z. *J. Phys. Chem.* **1993**, *99*, 4318−4326.
(31) Page, C. S.; Olivucci, M. *J. Comput. Chem.* **2002**, *24*, 298−309.
(32) Frisch, M. J.; Trucks, G. W.; Schlegel, H. B.; Scuseria, G. E.; Robb, M. A.; Cheeseman, J. R.; Zakrzewski, V. G.; Montgomery, J. A., Jr.; Stratmann, R. E.; Burant, J. C.; Dapprich, S.; Millam, J. M.; Daniels, A. D.; Kudin, K. N.; Strain, M. C.; Farkas, O.; Tomasi, J.; Barone, V.; Cossi, M.; Cammi, R.; Mennucci, B.; Pomelli, C.; Adamo, C.; Clifford, S.; Ochterski, J.; Petersson, G. A.; Ayala, P. Y.; Cui, Q.; Morokuma, K.; Malick, D. K.; Rabuck, A. D.; Raghavachari, K.; Foresman, J. B.; Cioslowski, J.; Ortiz, J. V.; Stefanov, B. B.; Liu, G.; Liashenko, A.; Piskorz, P.; Komaromi, I.; Gomperts, R.; Martin, R. L.; Fox, D. J.; Keith, T.; Al-Laham, M. A.; Peng, C. Y.; Nanayakkara, A.; Gonzalez, C.; Challacombe, M.; Gill, P. M. W.; Johnson, B. G.; Chen, W.; Wong, M. W.; Andres, J. L.; Head-Gordon, M.; Replogle, E. S.; Pople, J. A. *Gaussian 98*, revision A.7; Gaussian, Inc.: Pittsburgh, PA, 1998.
(33) Andersson, K.; Barisz, M.; Bernhardsson, A.; Blomberg, M. R. A.; Cooper, D. L.; Fleig, T.; Fülscher, M. P.; de Graaf, C.; Hess, B. A.; Karlström, G.; Lindh, R.; Malmqvist, P.-Å.; Neogrády, P.; Olsen, J.; Roos, B. O.; Schmmelpfennid, B.; Schültz, M.; Sadlej, A. J.; Schütz, M.; Seijo, L.; Serrano-Andrés, L.; Siegbahn, P. E. M.; Stårling, J.; Thorsteinsson, T.; Veryazov, V.; Widmark, P.-O. MOLCAS-5, version 5.1; University of Lund, Sweden, 2000.
(34) Robb, M. A.; Garavelli, M.; Olivucci, M.; Bernardi, F. In *Reviews in Computational Chemistry*; Lipkowitz, K. B., Boyd, D. B., Eds.; Wiley-VCH: New York, 2000; pp 87−146.
(35) Becker, R. S.; Favaro, G.; Gentili, P. L.; Romani, A.; Dias, F. M. B. *Chem. Phys.* **2005**, in press (doi: 10.1016/j.chemphys.2005.05.008).
(36) Ellis, G. P. *Chromenes, chromanones and chromones*; Wiley: New York, London, 1977.
(37) Reguero, M.; Olivucci, M.; Bernardi, F.; Robb, M. A. *J. Am. Chem. Soc.* **1994**, *116*, 2103−2144.
(38) Dushinsky, F. *Acta Physicochim. USSR* **1937**, *7*, 551−558.
(39) Favaro, G.; Romani, A.; Ortica, F. *Photochem. Photobiol. Sci.* **2003**, *2*, 1032−1037.
(40) Gentili, P. L.; Danilov, E.; Rodgers, M. A.; Ortica, F.; Favaro, G. *Photochem. Photobiol. Sci.* **2004**, *3*, 886−891.